RESEARCH ARTICLE
SPACE PHYSICS: IONOSPHERIC PHYSICS

Earth and Planetary Physics
9: 39–53, 2025
doi: 10.26464/epp2024014

The low-latitude sodium layer: comparative data from lidar observations at Hainan, China and São Paulo, Brazil

Fang Wu[1,2,3], Jing Jiao[1,2*], GuoTao Yang[1,2*], LiFang Du[1,2], ZhengKuan Liu[1,4], HaoRan Zheng[1,2], JiXin Guo[1,3], ShaoHua Gong[2,5], and YaJun Zhu[1,2]

[1]State Key Laboratory of Space Weather, National Space Science Center, Chinese Academy of Sciences, Beijing 100190, China;

[2]Hainan National Field Science Observation and Research Observatory for Space Weather, National Space Science Center, Chinese Academy of Sciences, Beijing 100190, China;

[3]University of Chinese Academy of Sciences, Beijing 100049, China;

[4]China-Brazil Joint Laboratory for Space Weather, NSSC/INPE, São José dos Campos 12227-010, Brazil;

[5]School of Physics and Electronics Engineering, Hainan Normal University, Haikou 571158, China

Key Points:

- Seasonal variations in the density of the Earth's Na layer exhibit similarities between hemispheres: both hemispheres display distinct annual (and weaker semi-annual) density variations. Density peaks generally occur near the equinoxes; minima are observed near the solstices.
- The Na layer over Brazil is normally denser than over Hainan Province, China, a difference that may be related to the South Atlantic Magnetic Anomaly (SAMA) or to the fountain effect.
- Nocturnal density variations within the Na layer over both of the two stations exhibit maxima that occur before sunrise.

Citation: Wu, F., Jiao, J., Yang, G. T., Du, L. F., Liu, Z. K., Zheng, H. R., Guo, J. X., Gong, S. H., and Zhu, Y. J. (2025). The low-latitude sodium layer: comparative data from lidar observations at Hainan, China and São Paulo, Brazil. *Earth Planet. Phys.*, *9*(1), 39–53. http://doi.org/10.26464/epp2024014

Abstract: Physical and chemical processes observed in the mesosphere and thermosphere above the Earth's low latitudes are complex and highly interrelated to activity in the low-latitude ionosphere. Metallic sodium detected by lidar can yield clues to dynamic and chemical processes in these spatial layers above the Earth's atmosphere. This paper is based on sodium layer data collected at two low-latitude stations, one in the northern hemisphere and one in the southern. The low-latitude sodium layer exhibits conspicuous seasonal variations in shape, density, and altitude; these variations are similar between Earth's hemispheres: sodium layer density at both stations reaches its seasonal maximum in autumn and minimum in summer. However, maximal Na density over Brazil is greater than that over Hainan. Nocturnal variations of Na density above the two low-latitude stations are also similar; at both, maxima are observed before sunrise. Some variations of the Na layer over Brazil that differ from those observed in the northern hemisphere may be related to the South Atlantic Magnetic Anomaly (SAMA) or fountain effect. We suggest that low-latitude Na layer data may provide useful additional evidence that could significantly improve the low-latitude part of the WACCM-Na model.

Keywords: metallic sodium layer; seasonal variation; nocturnal variation; lidar

1. Introduction

Layers of neutral metal elements — such as sodium (Na), iron (Fe), potassium (K), nickel (Ni), and calcium (Ca) — are found above Earth in the mesosphere and lower thermosphere (MLT) regions, normally located between 80 and 110 km above sea level. Most studies suggest that these metal atoms originate in meteoroids from outer space, which lose them through ablation during high velocity entry into Earth space (Megie et al., 1978; Plane, 2003; Plane et al., 2015). In addition to complex chemical cycling reactions with various atmospheric constituents, such as H, O, O_2 and O_3, these metal species also respond to a range of ionospheric activities and various scales of fluctuation and atmospheric turbulence, such as ionospheric disturbances, tidal waves, and gravity waves; thus, their spatial distributions exhibit various forms and different behavioral characteristics. Therefore, knowledge of changes in these metal layers can act as tracers of complex chemical and dynamic processes occurring in the MLT region (She CY et al., 2000; Xu JY and Smith, 2003).

Observation of metal layers has been ongoing for more than half a century. Sodium layers have been studied most extensively

First author: F. Wu, fwu@swl.ac.cn
Correspondence to: J. Jiao, jjiao@swl.ac.cn
G. T. Yang, gtyang@swl.ac.cn
Received 23 OCT 2023; Accepted 24 JAN 2024.
First Published online 18 APR 2024.

because their particle concentrations are large, their lifetimes long, and their backscatter cross-section characteristics make them easy to observe by means of high-quality echo signals. Bowman et al. (1969) first observed the Na layer with lidar. Since then, lidars have been widely used as the main means of observing the Na layer from global in-situ stations.

The Na layer is susceptible to chemical, dynamic, and ionospheric factors, which are reflected in long-term changes in its characteristic spatial parameters, such as column abundance, centroid height, and RMS width. Observations from multiple lidar stations at different latitudes show that the Na layer exhibits clear nocturnal and seasonal variations (e.g., Megie and Blamont, 1977; Simonich et al., 1979; Eska et al., 1998; Plane et al., 1999; Andrioli et al., 2020; She CY et al., 2000; Clemesha et al., 2003; Gardner et al., 2005; Friedman and Chu XZ, 2007; Yi F et al., 2009; Gong SH et al., 2013; Yue XC et al., 2017; Jiao J et al., 2022). Observations from the low-latitude São José dos Campos (23.1°S) station in the southern hemisphere have shown that the Na layer's column abundance reaches its maximum in winter, with occasional vertical down-transport structures of 1–4 km/h (Simonich et al., 1979). In recent years, Andrioli et al. (2020) has further reported on the local Na and K layers, based on 152 observation nights before February 2019, showing that Na density exhibits semi-annual changes between 80–91 km altitude, with maxima appearing around May and September; the centroid altitude exhibits annual changes, reaching its maximum at the equinoxes; column abundance exhibits annual changes, reaching its maximum between the equinoxes. Furthermore, they found that the Na layer exhibits the same vertical down-transport structure on 66% of nights and speculated that the structure is due to the sporadic E layer (Es), ion-neutral reactions, and strong shear winds pushing the metal layer downward. Results from the Hainan station (19.99°N) in the northern hemisphere are similar to those from other latitudes along 120°E in Beijing (40.47°N) and Hefei (31.87°N), with the difference that the Na layer's column abundance exhibits more semi-annual change in Hainan; maximum density is reached in winter and minimum in summer; the centroid height above Hainan exhibits more obvious semi-annual changes than are observed at other latitudes; no obvious seasonal change of RMS width is observed at Hainan (Gong SH et al., 2013). The Na layer's column abundance at Wuhan (30.5°N, 114.4°E) in the mid-latitude transition zone exhibits no obvious semi-annual changes, but does show strong annual changes (Yi F et al., 2009). The annual changes in the Na layer's column abundance in mid-latitude areas are stronger than those in lower latitudes. At Urbana, Illinois (40°N) and Fort Collins, Colorado (41°N), the Na layer's column abundance exhibits strong annual changes between 81–107 km, reaching its minimum in summer and maximum in winter, with a difference between the minimum and maximum values of about a factor of 4 (Plane et al., 1999). The maximum and minimum column abundances of the Na layer over Fort Collins were 6.0×10^{13} m^{-2} and 1.7×10^{13} m^{-2}, respectively, appearing in November and June, respectively (She CY et al., 2000). The column abundance of the Na layer over Antarctica exhibits severe annual changes, partly due to the consumption of Na in polar mesospheric clouds during summer (Plane, 2004; Gardner et al., 2005). In addition to detection by ground-based lidar, long-term changes of the Na layer can also be observed in data from instruments on satellites. Fussen et al. (2004, 2010) used measurement data from the GOMOS instrument on the ENVISAT satellite to show that changes in the Na layer shift from semi-annual to annual characteristics with increasing latitude. Hedin and Gumbel (2011) used data from the Optical Spectrograph and Infra-Red Imager System (OSIRIS) on the Odin satellite to confirm that the Na layer exhibits strong annual changes in mid-to-high latitudes, mainly due to higher winter temperatures in the MLT region, which lead to maximum annual Na density, and lower summer temperatures, which lead to Na depletion. They also pointed out that no obvious seasonal variation of the Na layer is observed in low-latitude areas. The global data show differences between the northern and southern hemispheres: Na column abundances are greater in the fall in the northern hemisphere, but are greater in the spring in the southern hemisphere. It should be noted that although satellites can observe the Na layer globally, they cannot provide uninterrupted observations of the same region throughout the night, so there has been a lack of research on diurnal variations of the Na layer; indeed, due to orbit and inclination limitations, there may be no satellite data for some latitudes and months.

It is generally believed that seasonal variations of the Na layer are related to temperature. Outside the tropical regions, the main reactions in the upper part (above 95 km) of the Na layer are ion-molecule reactions, which show only a weak negative correlation with temperature. Meanwhile, background temperature and wind field changes also affect the Na layer. Variations in the lower part (below 95 km) of the Na layer show significant positive correlation with temperature, mainly due to acceleration of reactions such as $NaHCO_3 + H \rightarrow Na + H_2CO_3$ under higher temperatures (Plane et al., 1999; Fan ZY et al., 2007).

In the past 20 years, a global atmospheric Na layer model called WACCM-Na (the Whole Atmosphere Community Climate Model with Na chemistry) has been developed based on observations and on related physical and chemical parameters in laboratory kinetic studies, using the CESM2 framework. This model can well reproduce, at most latitudes, the seasonal variation characteristics of the Na layer observed by satellite and ground-based lidar (Marsh et al., 2013; Dunker et al., 2015; Feng WH et al., 2017; Langowski et al., 2017; Li T et al., 2018; Yuan T et al., 2019; Danabasoglu et al., 2020). Dawkins et al. (2015) validated the WACCM-Na model using ERA-Interim data (2004–2013), showing that the Na layer exhibits a maximum in the southern hemisphere in spring (March–April) and less obvious hemispheric differences in autumn (September–October). Recently, the latest version of the model has again shown good agreement with long-term observations of the Na layer over Beijing (40.41°N, 116.01°E) (Jiao J et al., 2022).

Although there have been many studies of seasonal variation, there is a lack of research on long-term variation characteristics of the Na layer in the low-latitude regions of both the northern and southern hemispheres. In this study, we report on seasonal and nighttime variation characteristics of the low-latitude Na layer using data from the International Meridian Circle Program (IMCP). Our work is based on long-term monitoring results from two Na fluorescence lidars located in low latitudes of the northern hemi-

sphere (Haikou, China), and of the southern hemisphere (São Paulo, Brazil), respectively. Most studies have shown that seasonal variations of the Na layers are associated primarily with seasonal variations of temperatures at the mesopause (Plane et al., 2015), which would suggest a clear symmetrical distribution between the two hemispheres at 20°N and 20°S (Cao WX et al., 2012; Zhao XR et al., 2020).

However, the magnetic latitudes of the two stations are different; special phenomena in the ionosphere, such as ionospheric irregularities or the equatorial fountain effect, may thus have different effects on the lower ionospheres of the two hemispheres. In addition, the Brazilian station is located within the South Atlantic Magnetic Anomaly (SAMA) region; thus, the difference in magnetic strength between the two locations may also have an impact on the ionosphere, which may be mapped through effects on mean properties of the Na layer.

In this paper, we hope to establish reference results for future studies of the structure of low-latitude ionospheric irregularities, based on analysis of asymmetries between long-term variations of the Na layer at the two low-latitude locations, which could serve as a tracer of those irregularities. In Section 2, we introduce the Na fluorescence lidar system and density inversion method. In Section 3, we analyze and compare characteristics of seasonal variations of the Na layer densities and characteristic parameters in data from the two stations, and also discuss and analyze the diurnal (nighttime) variations observed over the composite years and composite months of data from the two stations.

2. Data and Methods

The two stations in Haikou, China (19.99°N, 110.34°E) and São José dos Campos, Brazil (23.1°S, 45.9°W) have similar lidar systems, based on the resonance fluorescence scattering mechanism of Na atoms. These devices emit a 1064 nm fundamental wave laser beam from an Nd: YAG solid-state laser, which is then pumped by a tunable dye laser to produce a yellow laser beam at 589 nm (close to the transition spectral line D_2 of Na atoms). The laser beam is injected vertically into the atmosphere through a beam expander and a coated full-reflection mirror. In the metal layer it excites Na atoms to emit resonance fluorescence scattering. Back on the ground, the scattered signal is received by a large-aperture Cassegrain coated telescope, and the signal data are digitized and stored using a photomultiplier tube and a photon counting card. The parameters of the lidar systems at the two stations are roughly the same, as shown in Table 1; more detailed parameters and system descriptions can be found in Gong SH et al. (2013) and Jiao J et al. (2018).

Observations of the Na layer over Haikou, China, at low latitudes in the northern hemisphere, were obtained from the Space Environment Ground-based Comprehensive Monitoring Network (i.e., the Meridian Project, http://data.meridianproject.ac.cn/); data describing the low latitude southern hemisphere Na layer over Brazil were provided by the São José dos Campos station. This study is based on single-night observations of duration greater than 3 hours, from both stations, as follows: from the Haikou station, we selected 300 observation nights between January 2017 and December 2020, a total of approximately 2552 hours; from the São José dos Campos station, 284 observations nights between January 2017 and November 2021, a total of approximately 2091 hours. Due to limited data availability, such as a data gap for Brazil from October 2019 to April 2021, we do not attempt to describe year-to-year variations. More details are included in the attached Figure S1 and Figure S2.

Andrioli et al. (2020) analyzed the average characteristics of the Na and K layers in Brazil using data from 152 valid observation nights, a total of 1230 hours of data, roughly 40% less than our comparable São José dos Campos station data (see Figure 1 for

Table 1. Main specifications of the Na fluorescence lidars at Hainan and Brazil.

	Hainan	Brazil
Transmitter wavelength (nm)	589	589
Pulse energy (mJ)	50	≥35
Pulse width (ns)	~10	~10
Repetition rate (Hz)	50	50
Receiver telescope diameter (mm)	~Φ1000	~Φ1000
Field of view (mrad)	0.2–2	≤1
Receiver filter wavelength (nm)	589	589
Bandwidth (nm)	1	1

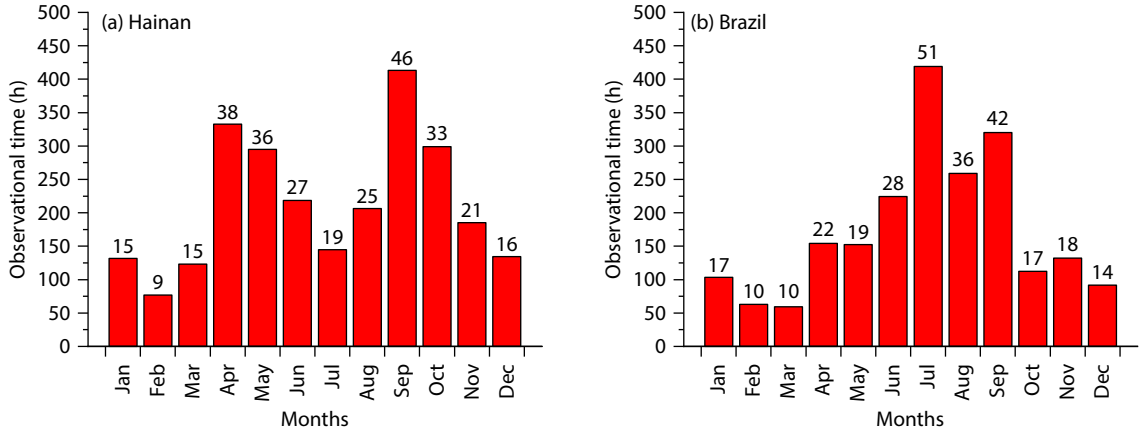

Figure 1. Histograms of the monthly observational hours and nights: (a) at Hainan; (b) at Brazil.

the effective monthly observation times in Haikou and São José dos Campos on which this study is based). During the summer months (June–August in Haikou and December–February in São José dos Campos), the monsoon and heavy rainfall affected operations of the lidar systems, so effective observation data for both stations during the summer months are relatively limited. And at Haikou in the winter, December–February, cloudy weather limited data collection. Nevertheless, at least 60 hours of data were collected in all months at both stations, providing sufficient sample size for this study. As shown in Figure S2, nighttime observation periods, from 21 LT to 04 LT, constitute more than 78% of total observations each month at both the Hainan and the Brazil stations. Therefore, we believe that the impact of data gaps on the results of the monthly averaging study will be small.

According to the contrast elimination of lidar equations of atmospheric Rayleigh scattering and Na resonance fluorescence scattering, the number density of Na atoms $n_{\mathrm{Na}}(z)$ can be expressed as (Chu XZ and Papen, 2005; Jiao J et al., 2015):

$$n_{\mathrm{Na}}(z) = n_{\mathrm{Ray}}(z_{\mathrm{Ray}}) \cdot \frac{\sigma_{\mathrm{Ray}}(\pi,\lambda)}{\sigma_{\mathrm{Na}}(\lambda)} \cdot \frac{z^2}{z_{\mathrm{Ray}}^2} \cdot \frac{N_s(\lambda,z) - N_B}{N_R(\lambda,z_R) - N_B}, \tag{1}$$

where z is the altitude, and z_{Ray} is the reference altitude (35 km for both stations). Atmospheric density at daily reference altitude can be found on NASA's official website (https://ccmc.gsfc.nasa.gov/modelweb/#atmo). As indicated in Table 1, laser pulse energies between the two stations are not identical. However, normalization of the denoised signal involves division by the photon counts at the selected reference altitude z_{Ray}, removing the influence of such energy differences. When the wavelength λ is 589 nm, the Rayleigh scattering cross section $\sigma_{\mathrm{Ray}}(\pi,\lambda)$ is 4.14×10^{-32} m^{2}sr^{-1}, and the Na atom effective scattering cross section $\sigma_{\mathrm{Na}}(\lambda)$ is 5.22×10^{-16} m^{2}sr^{-1} around 200 K. N_s and N_R are, respectively, the number of echo photons observed at altitudes z and z_{Ray}. N_B is the ambient background noise. For both stations, we selected N_B to be the average of echo photons detected between 140 and 160 km.

Na layer characteristics can be described by the parameters of Na layer peak density P_{Na}, column abundance C_{Na}, centroid height H_{Na}, and RMS width W_{Na}, which can reflect changes of the Na layer itself and interactions between the Na layer and atmospheric dynamics and chemical processes. We define m_i as the integral value of the density of Na in the range of about $\Delta z_0/2$ above and below the altitude z_0 (Gardner et al., 1986; Gong SS et al., 2003):

$$m_i = \int_{z_0-\Delta z_0/2}^{z_0+\Delta z_0/2} z^i n_{\mathrm{Na}}(z)\,\mathrm{d}z. \tag{2}$$

Generally we take z_0 = 90 km, Δz_0 = 30 km. Then each parameter can be expressed as:

$$C_{\mathrm{Na}} = m_0, \quad H_{\mathrm{Na}} = \frac{m_1}{m_0}, \quad W_{\mathrm{Na}} = \sqrt{\frac{m_2}{m_0} - \left(\frac{m_1}{m_0}\right)^2}. \tag{3}$$

The original temporal resolution of the observation data in Hainan is 20 s or 102 s, and the original spatial resolution is 96 m. The original resolution of the observations in Brazil is 20 s, 96 m. In order to reduce the error and improve the signal-to-noise ratio (SNR), we accumulated the observed data for 10 min in time, smoothing it for 1 km in altitude, then subtracted the average background noise, finally obtaining the Na layer density according to Formula (1). We then analyzed the characteristic parameters of Na density according to Formula (3).

3. Results and Discussion

3.1 Seasonal Variations

The seasonal variations of the composite monthly average Na density over Hainan from 2017 to 2020 and Brazil from 2017 to 2021 are shown in Figure 2. We can see that the Na layer peak density over Hainan reaches its maximum in October and April (near the equinoxes), with values of approximately 4018 cm^{-3} and 2493 cm^{-3}, respectively, and its minimum in the summer months (July, near the solstice) with a value of around 1913 cm^{-3}. The monthly average Na layer density over Brazil reaches its maximum of approximately 4330 cm^{-3} in April (near the autumnal equinox), with a secondary maximum of about 3613.6 cm^{-3} appearing in September (near the vernal equinox). The peak density is relatively small near the solstice (January, July, and December), with values

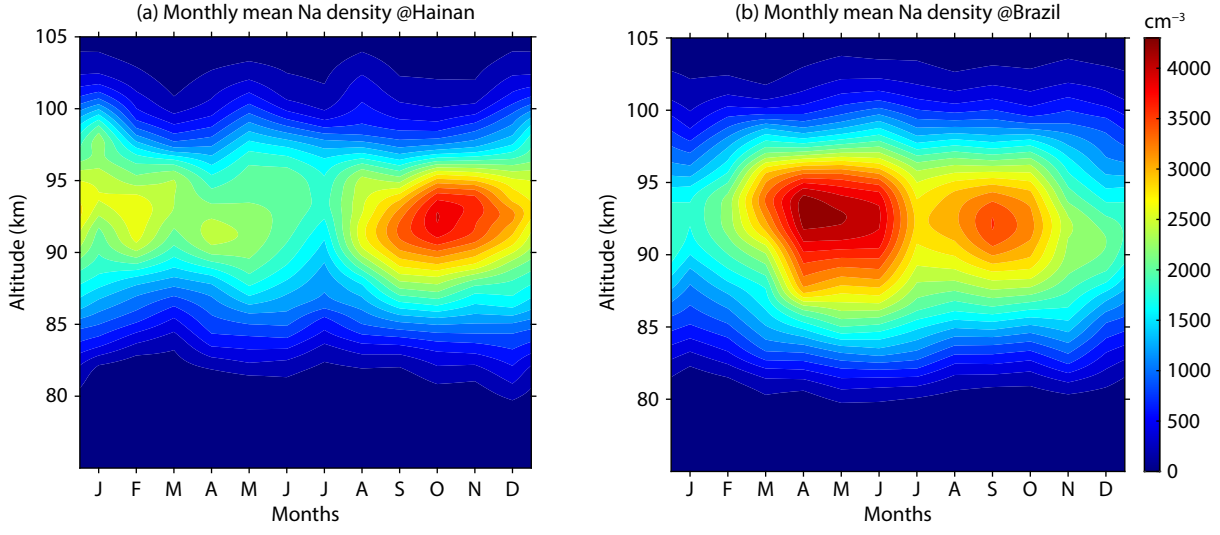

Figure 2. Comparison of seasonal variations of nocturnal Na density at Hainan (a) and Brazil (b).

of 1833 cm^{-3}, 2932 cm^{-3}, and 2203 cm^{-3}, respectively. These results indicate that both stations exhibit significant annual and weaker semi-annual variations in Na density, with the maximal density generally occurring near the equinoxes and the submaximal density near the solstices.

After seasonal averaging of the monthly data, as shown in Figure 3, the density profiles, as a function of altitude above both stations, exhibit a Gaussian distribution. Na layer average densities are lowest above both stations during their respective summer seasons, but the altitude of peak density within the layer over Hainan is slightly higher than the altitude of peak density over Brazil: Over Hainan, the altitude of peak density in summer (June–August) is 93.3 km, where the density is ~2215 cm^{-3}; over Brazil, peak density in summer (December–February) appears at 91.8 km, where the average density reaches ~2067 cm^{-3}. Over Hainan in winter (December–February), peak density of ~2819 cm^{-3} is reached at altitude 92.8 km; over Brazil (June–July), peak density of ~3363.86 cm^{-3} is observed at 92.9 km. Interestingly, the autumn peak density at both stations is higher than the winter density, which differs from previous studies and requires further investigation.

In order to identify the proportion of annual variation component and semi-annual variation component from the daily average data of the characteristic parameters of Na layer, the following harmonic function is used to fit the data (Gardner et al., 2011):

$$f(d) = A_0 + A_1\cos\frac{2\pi(d-d_1)}{365} + A_2\sin\frac{4\pi(d-d_2)}{365}, \quad (4)$$

where A_0 is the average amplitude, A_1 and d_1 are the amplitude and phase of the annual change (12 months), respectively. A_2 and d_2 are the amplitude and phase of the semi-annual change (6 months), respectively. Detailed values of each fitting parameter in Equation (4) are shown in Table 2.

Figure 4 depicts the averaged yearly cycles of four parameters of the Na layer, as determined by fitting harmonic functions of annual and semi-annual periods. It can be seen that shifting the data from Brazil by 6 months verifies that the Na layers observed at both locations are consistent in how they vary seasonally. Figure 4a displays 12-month curves of fitted peak density data. Over Hainan, the composite year's *average* peak Na layer density is 3723.6 cm^{-3}. From the fitting results, the amplitude of Hainan's annual peak density is 3600 cm^{-3}, with a variation component of 25.2%; the maximum density value of the annual function occurs on October 30th of the composite year. The maximum semi-annual value appears on April 24, with a variation component of 16.6%. The phase of the annual variation component thus leads the semi-annual component by 189 days. The fitted curve shows that peak density over Hainan exhibits significant annual and weaker semi-annual variation. Over Brazil, the annual average peak density is 3912.7 cm^{-3}. From the fitting results, the amplitude

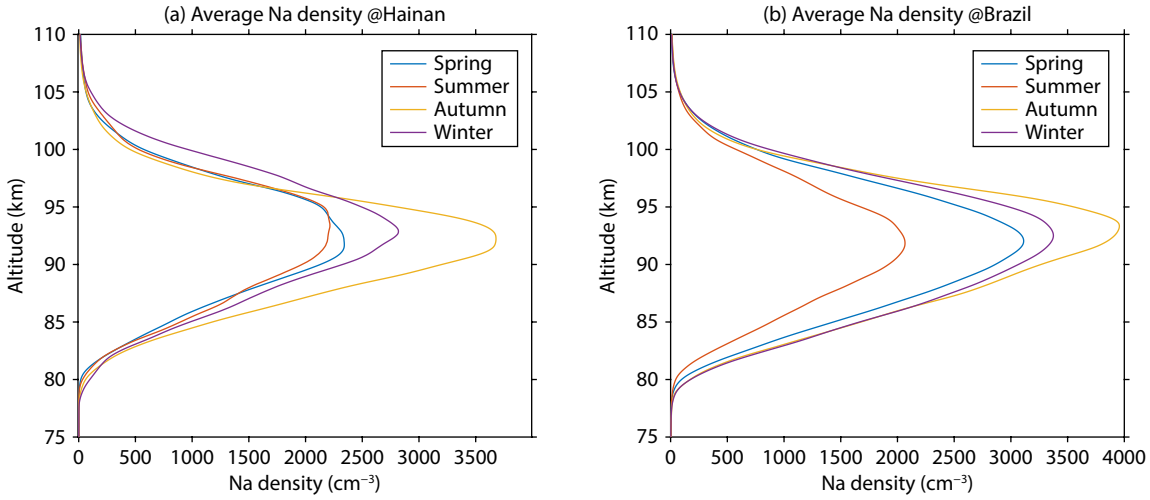

Figure 3. Altitude profiles of the seasonally-averaged Na layer density distributions observed at Hainan (a) and Brazil (b).

Table 2. Comparison of fitting parameters at Hainan (19.99°N) and Brazil (23.1°S).

		A_0	A_1	A_2	d_1 (Days)	d_2 (Days)	A_1/A_0	A_2/A_0
Peak density (×10^3 cm^{-3})	19.99°N	3.60	0.93	0.61	303	114	25.2%	16.6%
	23.1°S	4.02	1.00	1.03	160	111	24.9%	25.6%
Column abundance (×10^8 cm^{-2})	19.99°N	32.87	5.47	4.19	297	115	16.6%	12.8%
	23.1°S	39.90	10.82	8.21	170	115	27.1%	20.6%
Centroid height (km)	19.99°N	92.08	0.27	0.36	48	15	0.3%	0.4%
	23.1°S	91.63	0.15	0.29	55	69	0.2%	0.3%
RMS width (km)	19.99°N	4.42	0.15	0.27	132	180	3.3%	6.1%
	23.1°S	4.63	0.08	0.16	218	167	1.8%	3.4%

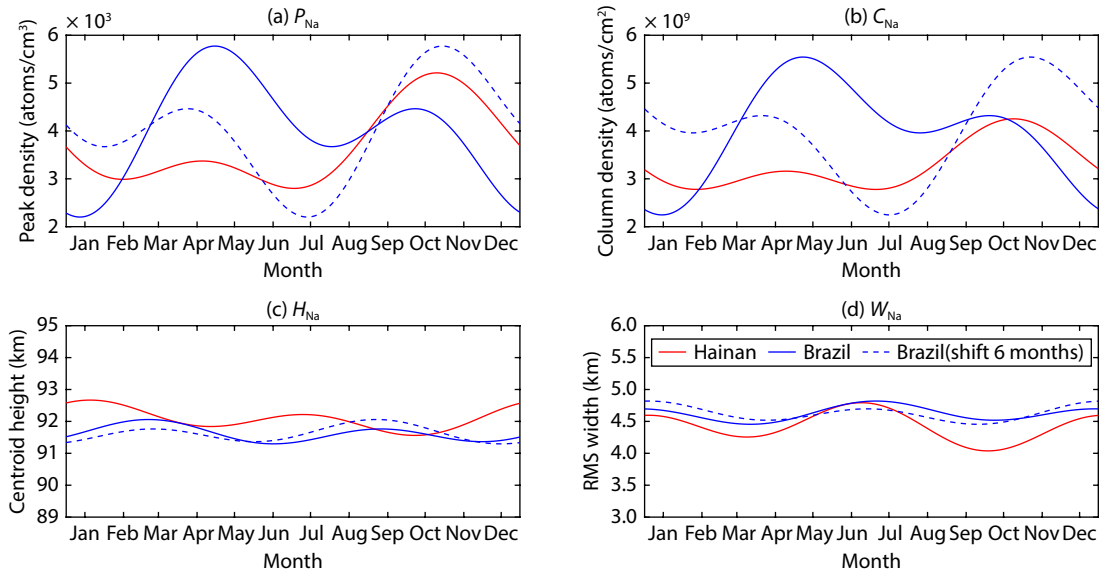

Figure 4. Comparison of Na layers over Hainan and Brazil: fitted curves of peak density (a), column abundance (b), centroid height (c) and RMS width (d).

of the annual harmonic function's peak density over Brazil is 4020 cm^{-3}, with an annual variation component of 24.9%; the maximum value occurs on June 9th of the composite year. The maximum value of the semi-annual harmonic function's component appears on April 21st; semi-annual variation component is 25.6%. The phase of the annual variation component thus leads the semi-annual component by 49 days. The fitted curve shows that the peak density over Brazil exhibits significant annual and semi-annual variation.

In Figure 4b, the annual average column abundance of the Na layer over Hainan is 3.23 × 10^9 cm^{-2}; over Brazil, it is 3.92 × 10^9 cm^{-2}. According to the fitting parameters in Table 2, the annual average amplitudes of the fitted Na layer column abundances over Hainan and Brazil are 3.29 × 10^9 cm^{-2} and 3.99 × 10^9 cm^{-2}, respectively, which are close to the observed mean values. In terms of amplitude, the annual and semi-annual variations of the Na layer over Hainan account for 16.6% and 12.8% of the total amplitude, respectively, both of which are lower than the annual variation component of 27.1% and semi-annual variation component of 20.6% over Brazil. In terms of phase, the annual and semi-annual variations of the Na layer over Hainan reach their maximum values on October 24 and April 25, respectively, while those over Brazil reach their maximum values on June 19 (near the summer solstice) and April 25, respectively. These results indicate that the annual and semi-annual variations of the Na layer column abundance over Brazil are more significant than those over Hainan; the locations of the maximum values are similar to the fitted peak density results.

In the observation data and fitting curve shown in Figure 4c, the average centroid height and fitting average value of Hainan are both 92.1 km, and the annual and semi-annual variations account for a small proportion, only 0.3% and 0.4% of the average amplitude throughout the year. The average centroid height and fitting average value of Brazil are both 91.6 km, and the annual and semi-annual variations also have a small proportion, accounting for 0.2% and 0.3%, respectively. In terms of phase, the maximum value of annual variation in Hainan appears on February 17, and the maximum value of semi-annual variation appears on January 15. The maximum value of annual variation in Brazil appears on February 24, and the maximum value of semi-annual variation appears on March 10. The annual and semi-annual variations of Hainan and Brazil have similar phases, with a difference of nearly two months in semi-annual variation. The above results indicate that the annual and semi-annual variations of the two stations are not significantly different; that semi-annual variation dominates; and that the centroid height of Hainan is generally higher than that of Brazil throughout the year.

As shown in Figure 4d, the mean RMS width above Hainan is 4.36 km, and 4.42 km is the average value after fitting. The maximum values of annual and semi-annual variations appear on May 12 and June 29, respectively, both of which are small, about 3.3% and 6.1%, respectively, with the semi-annual variation component 0.8 times higher than the annual variation component. The mean RMS width above Brazil is 4.36 km, and 4.65 km is the average value after fitting. The maximum values of annual and semi-annual variations appear on August 6 and June 16, respectively, both of which are small, about 1.8% and 3.4%, respectively, with the semi-annual variation component being about twice as high as the annual variation component. The average amplitude of the fitting curve of the two stations differs by 0.21 km, and the overall trend of change in both curves is similar. The characteristics of semi-annual and annual variations are not obvious; the RMS width at Brazil is larger than at Hainan throughout the year, but the fluctuation amplitude of the Hainan result is more significant than that for Brazil.

Based on the observation and fitting results of the two stations, we can draw the following conclusions: the peak density and column abundance of the two low-latitude stations in Hainan and Brazil show annual and semi-annual variations with differences in intensity; the centroid height and RMS width are relatively stable,

with small fluctuations over the months, and the characteristics of semi-annual variation are more obvious than those of annual variation.

3.2 Nocturnal Variations

Figure 5 shows the statistics of observation data in each hourly interval during the night for Hainan (LT = GMT + 8) and Brazil (LT = GMT – 3). It can be seen that the observation time for each interval in Hainan from 20:00 to 6:00 LT is not less than 40 hours, and the observation time at midnight 00:00 LT reaches 300 hours. In Brazil, the observation time for each interval from 19:00 to 5:00 LT is not less than 50 hours, and the observation time reaches 250 hours at 22:00 LT.

Figure 6 shows the composite nighttime observation map of Na density data (with a resolution of 10 minutes and 1 km) averaged for the same time period and height. It should be noted that the data for 19:00 LT in Hainan have been removed due to insufficient observations, and the data for 20:00 LT mostly come from autumn and winter. The nighttime data from 21:00 to 5:00 LT are evenly distributed. In Brazil, the data volume for spring and summer from 19:00 to 5:00 LT is relatively small, while the data for other time periods are evenly distributed. The results shown in Figure 6 have filtered-out the time periods with low observation volume; data volume for each interval is not less than 43 hours.

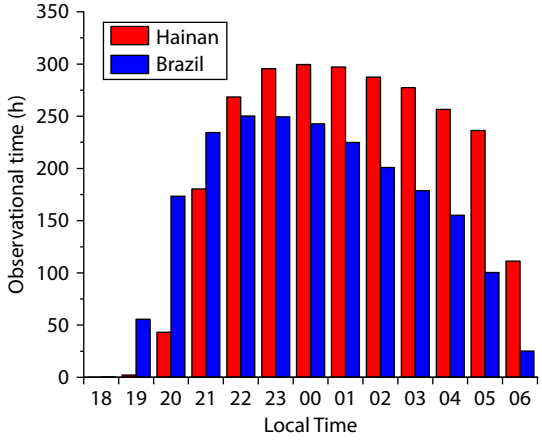

Figure 5. Histograms of observational times in each hour period at Hainan (red columns) and Brazil (blue columns).

In Figure 6, the peak Na density over Hainan gradually increases from 20:00 to 05:00 LT and reaches a maximum of 3398 cm^{-3} at 5:00 LT, while the peak height decreases from 92.5 km to 92.1 km with a descent rate of 0.04 km/h. The peak Na density in the composite nighttime observation of Brazil is smaller in the first half of the night than in the second half, and reaches a maximum of 4187 cm^{-3} at 02:00 LT. The peak height of the Na layer over Brazil decreases from 93.9 km to 91.6 km from 19:00 to 04:00 LT, with a descent rate of 0.25 km/h. However, it can be seen from Figure 6 that the descent rates over Haikou and Brazil are relatively close from 22:00 LT to 03:00 LT. Specifically, the peak height of Na layer decreases from 92.7 km to 92.0 km with a rate of 0.14 km/h over Hainan, while it descends from 92.7 km to 91.9 km with a rate of 0.16 km/h over Brazil. Furthermore, Na layers over both stations exhibit an ascent during nighttime peak hours. The peak height increases by 0.2 km/h from 20:00 LT to 22:00 LT and from 03:00 LT to 05:00 LT over Hainan. Similarly, the Na layer experiences an ascent with a rate of 1 km/h from 04:00 LT to 05:00 LT over Brazil. These variations may be attributed to other influencing factors, which will be explored in our next work.

To better analyze the nighttime variation characteristics of the Na layer, in Figure 7 we present the nighttime variations of each composite month from 19:00 to 05:00 LT for both stations. Time periods less than 3 hours in each month are not included in the plot. It can be seen from Figure 7a that the Na density over Hainan

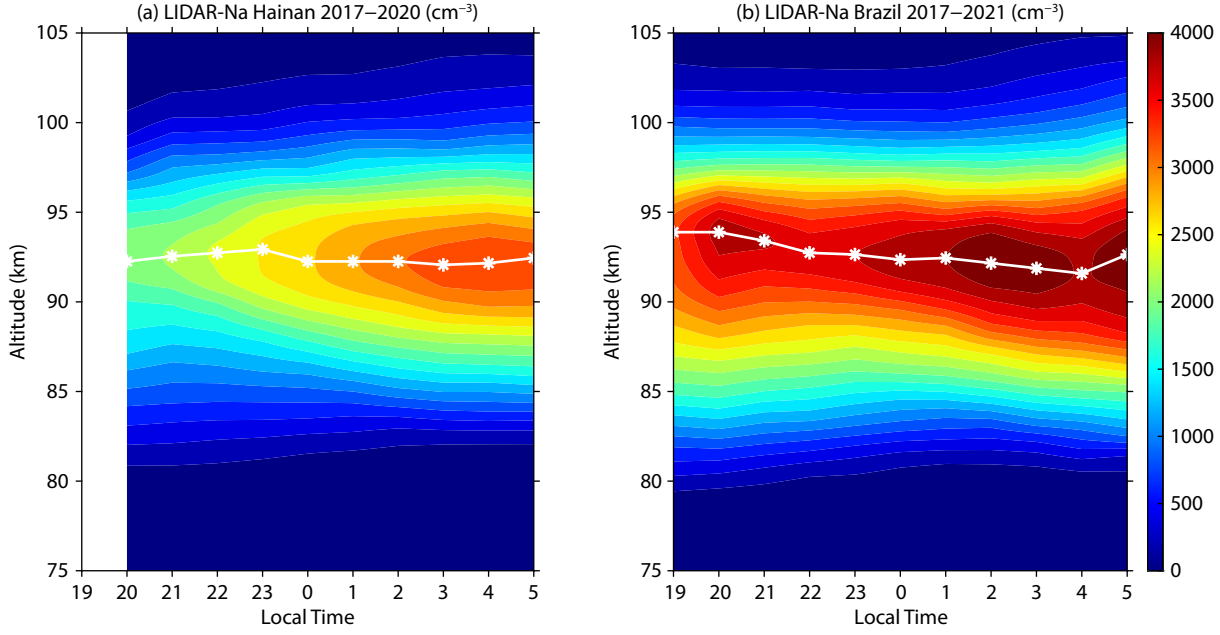

Figure 6. Comparison of annual composite night of the Na density at Hainan (a) and Brazil (b), the white asterisks indicate the altitude of peak Na density.

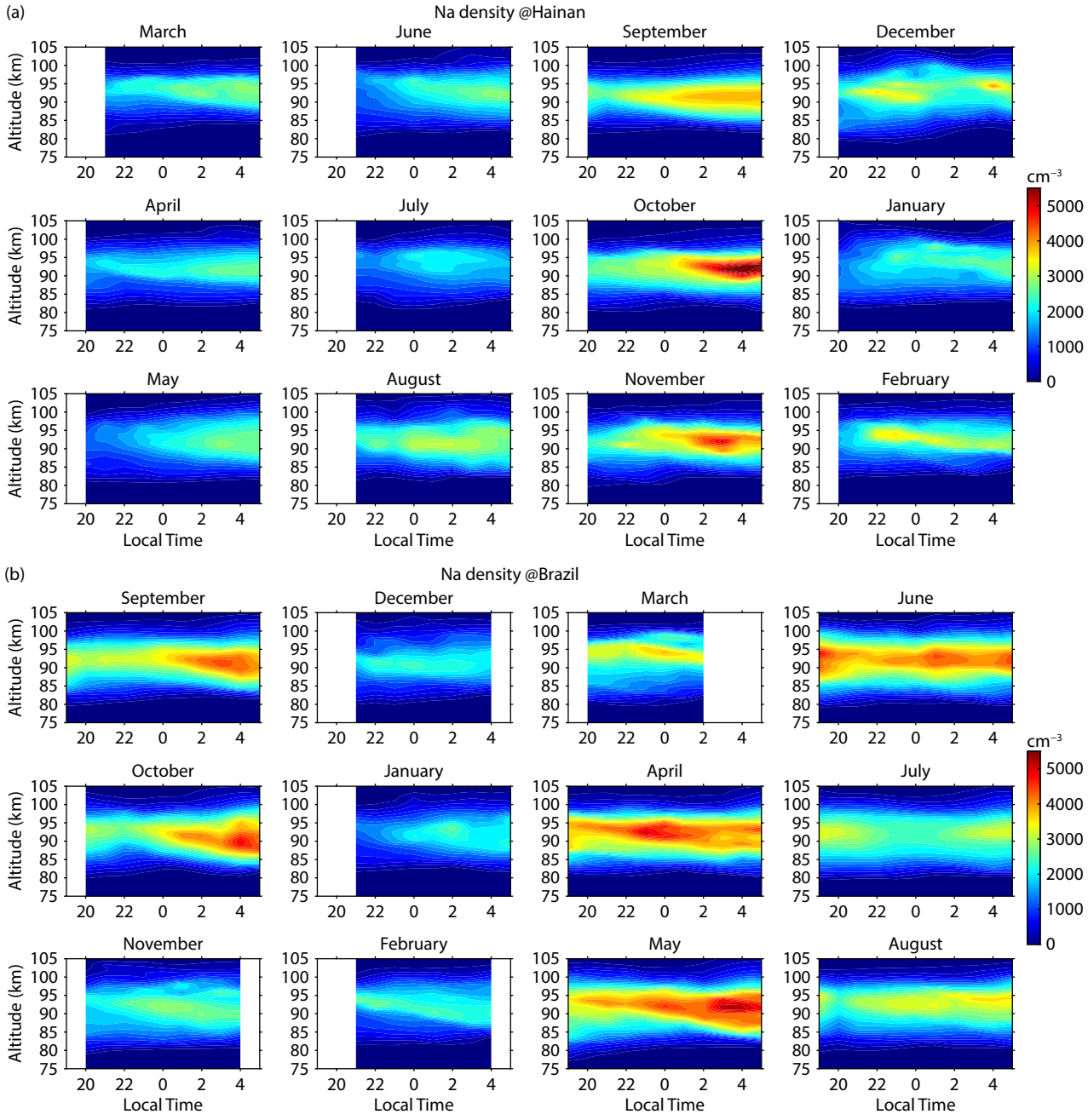

Figure 7. Comparison of monthly composite night observations of the Na density at Hainan (a) and Brazil (b). Each column in each panel from left to right represents spring, summer, autumn and winter.

is higher in months near the autumnal equinox (September and October) and lower in months near the summer solstice (June and July), while the Na density over Brazil is higher in months near the vernal equinox and autumnal equinox (April and September) and lower in months near the winter solstice and summer solstice (January, July, and December). These results show that the two stations have distinct annual variation characteristics, and that the semi-annual variation characteristics over Brazil are more significant than those over Hainan, which verifies the conclusions of Section 3.1 regarding seasonal variations.

As shown in Figure 7, in most months the altitude of overnight peak Na density over Hainan and Brazil gradually moves downward with time. The same phase shift phenomenon is observed in the nighttime temperature and K layer over Arecibo station (18.35°N, 66.75°W) at low latitudes, which is attributed to the influence of periodic atmospheric waves such as tidal waves by Friedman and Chu XZ (2007) and Yue XC et al. (2017) because most non-coherent waves such as gravity waves have been smoothed out in the annual composite night averaging process, leaving mainly coherent waves synchronized with the diurnal cycle and its harmonics. Similar to the results of the annual composite nighttime observations, both Hainan and Brazil have eight months with significant density increases before dawn. Further studies are required in the future.

4. Discussion

4.1 Influence of Ionospheric Fountain Effect or SAMA

Existing research predominantly indicates that temperature changes at the mesopause are the primary influence on seasonal variations in the Na layer (Plane et al., 2015). However, it is noteworthy that the long-term trend in mesopause temperature becomes statistically insignificant at 20°N and 20°S, revealing a distinct symmetrical distribution of temperature between the two hemispheres (Cao WX et al., 2012; Zhao XR et al., 2020). Figure 2 and Figure 3 reveal that the Na density at Brazil is normally higher at each of the four seasons than at Hainan. This systematic difference contradicts the expected symmetrical distribution based on temperature alone. Therefore, we consider attributing this dissimilarity to variances in magnetic latitude: 10.47°N for Hainan and 27.19°S for Brazil.

Different magnetic latitudes lead to distinct ionospheric structures. As referenced in previous studies, we considered the transport effects of the equatorial fountain in our analysis. The equatorial fountain effect is two peaks at ±15° off the equator in the magnetic equator of the TEC distribution (Carter and Forbes, 1999; Bishop and Earle, 2003; Gao et al., 2015). Both models and observations confirm that the metal ions deposited from equatorial regions to low latitudes by the equatorial fountain effect contribute to Na^+ ions in the mesopause and thermosphere. Hainan is closer to the magnetic latitude where Na^+ is transported downward, making it more favorable for the formation of a denser Na layer compared to Brazil. However, as seen in Figure 2 and Figure 3, the normal Na density in Brazil is higher than in Hainan. Therefore, we attribute the impact of ion transport by the equatorial fountain effect to be less significant.

Apart from the magnetic latitude difference, the Brazil station is located in the SAMA region, characterized by a negative magnetic anomaly, markedly different from the expected symmetric dipole. The weak magnetic field in this region makes Brazil more susceptible to intrusion of energetic particles. Greater energetic particle precipitation leads to regular ionization sources that cause frequent nighttime Es occurrences, even during geomagnetically quiet periods (Abdu et al., 2005; Conceição-Santos et al., 2019). Additionally, some particles precipitate into the lower atmosphere and excite atoms/molecules during geomagnetically quiet periods (He F et al., 2020). Thus, we speculate that such particles precipitate into the atmosphere, resulting in increased nighttime Es layers and neutralization to form the Na layer over Brazil. Meanwhile, this effect is more pronounced than the impact of the equatorial fountain, leading to higher average Na densities at Brazil compared to Hainan.

4.2 Correlation Between Seasonal Patterns of Es Layer and Na Layers

As shown in Figure 2, our analysis reveals that both low-latitude stations exhibit distinct annual and weaker semi-annual variations of Na density, with maximum occurring near the equinoxes and minimum near the solstices. In contrast to our results, previous observations of E region irregularities/Es have shown a higher occurrence frequency during summer and autumn (Gong Y et al., 2007; Arras et al., 2008; Haldoupis, 2011; Chu YH et al., 2014; Resende et al., 2018). This difference can be attributed to the fact that the seasonal variations in Na density are primarily influenced by changes in the temperature at the mesopause (Fan ZY et al., 2007; Plane et al., 2015), rather than the occurrence rate of Es. To elucidate the distinctions, we compared the monthly average temperatures between the two stations using the Whole Atmosphere Community Climate Model WACCM model (Danabasoglu et al., 2020). As illustrated in Figure S3, the model simulates lower temperatures in the summer months (75–100 km) at both stations. The key chemical reaction for Na layer formation, $NaHCO_3 + H \rightarrow Na + H_2CO_3$, exhibits a slower reaction rate at lower temperatures, leading to reduced Na layer density during the summer (Plane et al., 2015). However, when Es layer occurrences are higher in autumn, the influence of neutralization of metal ions, $Na^+ + e^- \rightarrow Na + h\nu$, in the Es layer becomes more pronounced than the effect of temperature variations at the mesopause. This contributes to an increase in the density of Na layer during autumn. In summary, the different seasonal patterns between the Na layer density and the Es layer can be attributed to whether metal ion neutralization in the Es layer is the dominant factor.

4.3 Influence of Tides on the Na Layer's Summer Peak Height Discrepancy

As shown in Figure 3, the peak height of the Na layer over Haikou (93.3 km) is greater in the summer months than that of the Na layer over São Paulo (91.8 km). This difference may be attributed to tides-driven factors. To verify this claim, we reconstructed the horizontal wind field with all the tidal components provided by the Climatological Tidal Model of the Thermosphere (CTMT) (Oberheide et al., 2011), as shown in Figure 8. More complete monthly tides for the two locations are shown in Figure S4. The heights of horizontal wind shear generated over Hainan at 75–105 km, including both meridional and zonal winds, are greater than those above Brazil for most of the time during the summer months; higher wind shear altitudes over Hainan cause Na atoms or ions to converge at greater heights than over Brazil, explaining the observed altitude difference of 1.5 km between the monthly mean Na densities of the two stations.

5. Summary

This study compares observation data of the Na layer from 300 observation nights in Hainan and 284 observation nights in Brazil based on the lidars at the two low-latitude stations on the International Meridian. Using the density inversion method, we analyze and compare seasonal variation characteristics of the Na layer density at the two low-latitude stations. Observations of the Na layer above both Hainan and Brazil reveal distinct annual and weaker semi-annual variation characteristics; maximal Na density generally occurs near the equinoxes, minimum density occurs near the solstices. By analyzing seasonal variation characteristics of the featured parameters of data from the two stations, we report that the peak Na densities above the two stations exhibit distinct annual variation and slightly weaker semi-annual variation trends, but the semi-annual variation above Hainan is smaller than that observed above Brazil. The semi-annual variation dominates, and the position of the maximum density is similar to the fitting result of the peak density. The annual and semi-annual variations of the centroid height at both stations are not significant, and the semi-annual variation dominates. The centroid height over

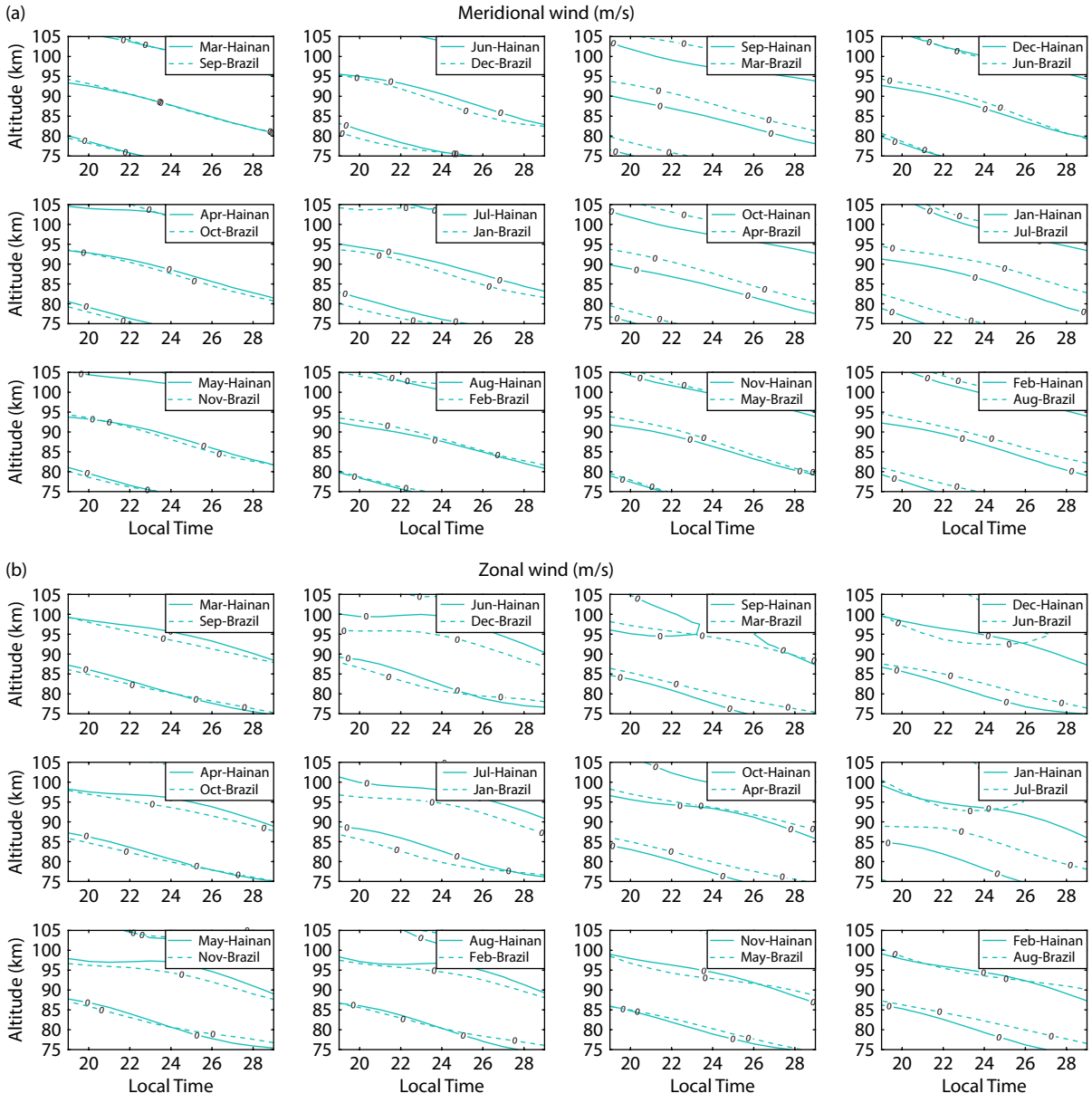

Figure 8. Comparison of monthly mean wind fields reconstructed from CTMT tidal components: (a) meridional wind and (b) zonal winds. Each column in each panel from left to right represents spring, summer, autumn and winter.

Hainan is generally higher than that over Brazil throughout the year. The RMS width variation is relatively stable, and the overall trend at both stations is similar. The RMS width over Brazil is larger than that over Hainan throughout the year, but the fluctuation amplitude over Hainan is more significant than that over Brazil. We also construct composite nighttime data for both stations for the entire year and for each month, and find that the peak Na density altitude over both stations gradually trends downward overnight with time, which trend is similar to nighttime temperature and K layer observations over the Arecibo station. This pattern is most likely caused by periodic atmospheric waves such as tidal waves. In addition, data from both Hainan and Brazil show a significant Na density increase before dawn in most months; the mechanism of this phenomenon needs further study. In future work, we will complement our observations by data from the new calcium ion lidar at Fuke, Hainan Island, China (19.5°N, 109.1°E), monitoring sodium atoms and calcium ion layers simultaneously. By using ionosondes or other ionosphere devices to capture unique phenomena associated with ionospheric irregularities, in conjunction with such studies of long-term variations of these two metal atoms and ions, we aim to gain insights into the structure of low-latitude ionospheric irregularities.

Acknowledgments

This work was supported by the NSFC (42374204, 42004143, 42364012), the Project of Stable Support for Youth Team in Basic Research Field, Chinese Academy of Sciences (Grant No. YSBR-018), the Scientific Projects of Hainan Province (KJRC2023C05, ZDYF2021GXJS040), the Innovational Fund for Scientific and Technological Personnel of Hainan Province, the Chinese Meridian Project, and Pandeng Program of National Space Science Center, Chinese Academy of Sciences. The Climato-

logical Tidal Model of the Thermosphere (CTMT) data were downloaded from the Clemson University website (https://globaldynamics.sites.clemson.edu/articles/ctmt.html). We also thank NCAR for providing the WACCM model outputs.

References

Abdu, M. A., Batista, I. S., Carrasco, A. J., and Brum, C. G. M. (2005). South Atlantic magnetic anomaly ionization: A review and a new focus on electrodynamic effects in the equatorial ionosphere. *J. Atmos. Solar-Terr. Phys.*, *67*(17-18), 1643–1657. https://doi.org/10.1016/j.jastp.2005.01.014

Andrioli, V. F., Xu, J., Batista, P. P., Pimenta, A. A., Resende, L. C. A., Savio, S., Fagundes, P. R., Yang, G., Jiao, J., … Liu, Z. (2020). Nocturnal and seasonal variation of Na and K layers simultaneously observed in the MLT region at 23°S. *J. Geophys. Res.: Space Phys.*, *125*(3), e2019JA027164. https://doi.org/10.1029/2019JA027164

Arras, C., Wickert, J., Beyerle, G., Heise, S., Schmidt, T., and Jacobi, C. (2008). A global climatology of ionospheric irregularities derived from GPS radio occultation. *Geophys. Res. Lett.*, *35*(14), L14809. https://doi.org/10.1029/2008GL034158

Bishop, R. L., and Earle, G. D. (2003). Metallic ion transport associated with midlatitude intermediate layer development. *J. Geophys. Res.: Space Phys.*, *108*(A1), 1019. https://doi.org/10.1029/2002JA009411

Bowman, M. R., Gibson, A. J., and Sandford, M. C. W. (1969). Atmospheric sodium measured by a tuned laser radar. *Nature*, *221*(5179), 456–457. https://doi.org/10.1038/221456a0

Cao, W. X., Zhang, S. D., Yi, F., and Huang, C. M. (2012). Variation of the mesopause observed by SABER/TIMED satellite. *Chinese J. Geophys. (in Chinese)*, *55*(8), 2489–2497. https://doi.org/10.6038/j.issn.0001-5733.2012.08.001

Carter, L. N., and Forbes, J. M. (1999). Global transport and localized layering of metallic ions in the upper atmosphere. *Ann. Geophys.*, *17*(2), 190–209. https://doi.org/10.1007/s00585-999-0190-6

Chu, X. Z., and Papen, G. (2005). Resonance fluorescence Lidar for measurements of the middle and upper atmosphere. In T. Fujii, et al. (Eds.), *Laser Remote Sensing* (pp. 179-432). Boca Raton: CRC Press.

Chu, Y. H., Wang, C. Y., Wu, K. H., Chen, K. T., Tzeng, K. J., Su, C. L., Feng, W., and Plane, J. M. C. (2014). Morphology of sporadic *E* layer retrieved from COSMIC GPS radio occultation measurements: Wind shear theory examination. *J. Geophys. Res.: Space Phys.*, *119*(3), 2117–2136. https://doi.org/10.1002/2013JA019437

Clemesha, B. R., Batista, P. P., and Simonich, D. M. (2003). Long-term variations in the centroid height of the atmospheric sodium layer. *Adv. Space Res.*, *32*(9), 1707–1711. https://doi.org/10.1016/S0273-1177(03)90466-2

Conceição-Santos, F., Muella, M. T. A. H., Resende, L. C. A., Fagundes, P. R., Andrioli, V. F., Batista, P. P., Pillat, V. G., and Carrasco, A. J. (2019). Occurrence and modeling examination of sporadic-*E* layers in the region of the South America (Atlantic) magnetic anomaly. *J. Geophys. Res.: Space Phys.*, *124*(11), 9676–9694. https://doi.org/10.1029/2018JA026397

Danabasoglu, G., Lamarque, J. F., Bacmeister, J., Bailey, D. A., DuVivier, A. K., Edwards, J., Emmons, L. K., Fasullo, J., Garcia, R., … Strand, W. G. (2020). The community earth system model version 2 (CESM2). *J. Adv. Model. Earth Syst.*, *12*(2), e2019MS001916. https://doi.org/10.1029/2019MS001916

Dawkins, E. C. M., Plane, J. M. C., Chipperfield, M. P., and Feng, W. (2015). The near-global mesospheric potassium layer: Observations and modeling. *J. Geophys. Res.: Atmos.*, *120*(15), 7975–7987. https://doi.org/10.1002/2015JD023212

Dunker, T., Hoppe, U. P., Feng, W. H., Plane, J. M. C., and Marsh, D. R. (2015). Mesospheric temperatures and sodium properties measured with the ALOMAR Na lidar compared with WACCM. *J. Atmos. Solar-Terr. Phys.*, *127*, 111–119. https://doi.org/10.1016/j.jastp.2015.01.003

Eska, V., Höffner, J., and von Zahn, U. (1998). Upper atmosphere potassium layer and its seasonal variations at 54°N. *J. Geophys. Res.: Space Phys.*, *103*(A12), 29207–29214. https://doi.org/10.1029/98JA02481

Fan, Z. Y., Plane, J. M. C., Gumbel, J., Stegman, J., and Llewellyn, E. J. (2007). Satellite measurements of the global mesospheric sodium layer. *Atmos. Chem. Phys.*, *7*(15), 4107–4115. https://doi.org/10.5194/acp-7-4107-2007

Feng, W. H., Kaifler, B., Marsh, D. R., Höffner, J., Hoppe, U. P., Williams, B. P., and Plane, J. M. C. (2017). Impacts of a sudden stratospheric warming on the mesospheric metal layers. *J. Atmos. Solar-Terr. Phys.*, *162*, 162–171. https://doi.org/10.1016/j.jastp.2017.02.004

Friedman, J. S., and Chu, X. Z. (2007). Nocturnal temperature structure in the mesopause region over the Arecibo Observatory (18.35°N, 66.75°W): Seasonal variations. *J. Geophys. Res.: Atmos.*, *112*(D14), D14107. https://doi.org/10.1029/2006JD008220

Fussen, D., Vanhellemont, F., Bingen, C., Kyrölä, E., Tamminen, J., Sofieva, V., Hassinen, S., Seppälä, A., Verronen, P., … Saavedra, R. (2004). Global measurement of the mesospheric sodium layer by the star occultation instrument GOMOS. *Geophys. Res. Lett.*, *31*(24), L24110. https://doi.org/10.1029/2004GL021618

Fussen, D., Vanhellemont, F., Tétard, C., Mateshvili, N., Dekemper, E., Loodts, N., Bingen, C., Kyrölä, E., Tamminen, J., … She, C. Y. (2010). A global climatology of the mesospheric sodium layer from GOMOS data during the 2002-2008 period. *Atmos. Chem. Phys.*, *10*(19), 9225–9236. https://doi.org/10.5194/acp-10-9225-2010

Gao, Q., Chu, X. Z., Xue, X. H., Dou, X. K., Chen, T. D., and Chen, J. S. (2015). Lidar observations of thermospheric Na layers up to 170 km with a descending tidal phase at Lijiang (26.7°N, 100.0°E), China. *J. Geophys. Res.: Space Phys.*, *120*(10), 9213–9220. https://doi.org/10.1002/2015JA021808

Gardner, C. S., Voelz, D. G., Sechrist, C. F. Jr., and Segal, A. C. (1986). Lidar studies of the nighttime sodium layer over Urbana, Illinois: 1. Seasonal and nocturnal variations. *J. Geophys. Res.: Space Phys.*, *91*(A12), 13659–13673. https://doi.org/10.1029/JA091iA12p13659

Gardner, C. S., Plane, J. M. C., Pan, W. L., Vondrak, T., Murray, B. J., and Chu, X. Z. (2005). Seasonal variations of the Na and Fe layers at the South Pole and their implications for the chemistry and general circulation of the polar mesosphere. *J. Geophys. Res.: Atmos.*, *110*(D10), D10302. https://doi.org/10.1029/2004JD005670

Gardner, C. S., Chu, X. Z., Espy, P. J., Plane, J. M. C., Marsh, D. R., and Janches, D. (2011). Seasonal variations of the mesospheric Fe layer at Rothera, Antarctica (67.5°S, 68.0°W). *J. Geophys. Res.: Atmos.*, *116*(D2), D02304. https://doi.org/10.1029/2010JD014655

Gong, S. H., Yang, G. T., Xu, J. Y., Xue, X. H., Jiao, J., Tian, D. W., Guan, S., and Liu, Z. K. (2013). Nighttime and seasonal variations of the sodium layer measured by Lidar at different latitudes in China. *Chinese J. Geophys.*, *56*(4), 361–372. https://doi.org/10.1002/cjg2.20035

Gong, S. S., Yang, G. T., Wang, J. M., Cheng, X. W., Li, F. Q., and Wan, W. X. (2003). A double sodium layer event observed over Wuhan, China by lidar. *Geophys. Res. Lett.*, *30*(5), 1209. https://doi.org/10.1029/2002GL016135

Gong, Y., Shi, J. K., and Wang, G. J. (2007). Investigation on properties of ionospheric Es layer in Hainan region. *Chin. J. Space Sci. (in Chinese)*, *27*(3), 198–203. https://doi.org/10.11728/cjss2007.03.198

Haldoupis, C. (2011). A tutorial review on sporadic *E* layers. In M. A. Abdu, et al. (Eds.), *Aeronomy of the Earth's Atmosphere and Ionosphere* (pp. 381-394). Dordrecht: Springer. https://doi.org/10.1007/978-94-007-0326-1_29

He, F., Wei, Y., and Wan, W. X. (2020). Equatorial aurora: the aurora-like airglow in the negative magnetic anomaly. *Natl. Sci. Rev.*, *7*(10), 1606–1615. https://doi.org/10.1093/nsr/nwaa083

Hedin, J., and Gumbel, J. (2011). The global mesospheric sodium layer observed by Odin/OSIRIS in 2004-2009. *J. Atmos. Solar-Terr. Phys.*, *73*(14-15), 2221–2227. https://doi.org/10.1016/j.jastp.2010.10.008

Jiao, J., Yang, G. T., Wang, J. H., Cheng, X. W., Li, F. Q., Yang, Y., Gong, W., Wang, Z. L., Du, L. F., … Gong, S. S. (2015). First report of sporadic *K* layers and comparison with sporadic Na layers at Beijing, China (40.6°N, 116.2°E). *J. Geophys. Res.: Space Phys.*, *120*(6), 5214–5225. https://doi.org/10.1002/2014JA020955

Jiao, J., Yang, G. T., Cheng, X. W., Liu, Z. K., Wang, J. H., Yan, Z. Z., Wang, C., Batista, P., Pimenta, A., … Denardini, C. M. (2018). Simultaneous lidar observation of peculiar sporadic K and Na layers at São José dos Campos (23.1°S, 45.9°W), Brazil. *Adv. Space Res.*, *61*(7), 1942–1951. https://doi.org/10.1016/j.asr.2017.12.002

Jiao, J., Feng, W. H., Wu, F., Wu, F. J. Zheng, H. R., Du, L. F., Yang, G. T., and Plane, J. (2022). A comparison of the midlatitude nickel and sodium layers in the mesosphere: Observations and modeling. *J. Geophys. Res.: Space Phys.*, *127*(2), e2021JA030170. https://doi.org/10.1029/2021JA030170

Langowski, M. P., von Savigny, C., Burrows, J. P., Fussen, D., Dawkins, E. C. M., Feng, W. H., Plane, J. M. C., and Marsh, D. R. (2017). Comparison of global datasets of sodium densities in the mesosphere and lower thermosphere from GOMOS, SCIAMACHY and OSIRIS measurements and WACCM model simulations from 2008 to 2012. *Atmos. Meas. Tech.*, *10*(8), 2989–3006. https://doi.org/10.5194/amt-10-2989-2017

Li, T., Ban, C., Fang, X., Li, J., Wu, Z. P., Feng, W. H., Plane, J. M. C., Xiong, J. G., Marsh, D. R., … Dou, X. K. (2018). Climatology of mesopause region nocturnal temperature, zonal wind and sodium density observed by sodium lidar over Hefei, China (32°N, 117°E). *Atmos. Chem. Phys.*, *18*(16), 11683–11695. https://doi.org/10.5194/acp-18-11683-2018

Marsh, D. R., Janches, D., Feng, W. H., and Plane, J. M. C. (2013). A global model of meteoric sodium. *J. Geophys. Res.: Atmos.*, *118*(19), 11442–11452. https://doi.org/10.1002/jgrd.50870

Megie, G., and Blamont, J. E. (1977). Laser sounding of atmospheric sodium interpretation in terms of global atmospheric parameters. *Planet. Space Sci.*, *25*(12), 1093–1109. https://doi.org/10.1016/0032-0633(77)90085-X

Megie, G., Bos, F., Blamont, J. E., and Chanin, M. L. (1978). Simultaneous nighttime Lidar measurements of atmospheric sodium and potassium. *Planet. Space Sci.*, *26*(1), 27–35. https://doi.org/10.1016/0032-0633(78)90034-X

Oberheide, J., Forbes, J. M., Zhang, X., and Bruinsma, S. L. (2011). Climatology of upward propagating diurnal and semidiurnal tides in the thermosphere. *J. Geophys. Res.: Space Phys.*, *116*(A11), A11306. https://doi.org/10.1029/2011JA016784

Plane, J. M. C., Gardner, C. S., Yu, J. R., She, C. Y., Garcia, R. R., and Pumphrey, H. C. (1999). Mesospheric Na layer at 40°N: Modeling and observations. *J. Geophys. Res.: Atmos.*, *104*(D3), 3773–3788. https://doi.org/10.1029/1998JD100015

Plane, J. M. C. (2003). Atmospheric chemistry of meteoric metals. *Chem. Rev.*, *103*(12), 4963–4984. https://doi.org/10.1021/cr0205309

Plane, J. M. C. (2004). A time-resolved model of the mesospheric Na layer: Constraints on the meteor input function. *Atmos. Chem. Phys.*, *4*(3), 627–638. https://doi.org/10.5194/acp-4-627-2004

Plane, J. M. C., Feng, W. H., and Dawkins, E. C. M. (2015). The mesosphere and metals: chemistry and changes. *Chem. Rev.*, *115*(10), 4497–4541. https://doi.org/10.1021/cr500501m

Resende, L. C. A., Arras, C., Batista, I. S., Denardini, C. M., Bertollotto, T. O., and Moro, J. (2018). Study of sporadic E layers based on GPS radio occultation measurements and digisonde data over the Brazilian region. *Ann. Geophys.*, *36*(2), 587–593. https://doi.org/10.5194/angeo-36-587-2018

She, C. Y., Chen, S. S., Hu, Z. L., Sherman, J., Vance, J. D., Vasoli, V., White, M. A., Yu, J. R., and Krueger, D. A. (2000). Eight-year climatology of nocturnal temperature and sodium density in the mesopause region (80 to 105 km) over Fort Collins, Co (41°N, 105°W). *Geophys. Res. Lett.*, *27*(20), 3289–3292. https://doi.org/10.1029/2000GL003825

Simonich, D. M., Clemesha, B. R., and Kirchhoff, V. W. J. H. (1979). The mesospheric sodium layer at 23°S: Nocturnal and seasonal variations. *J. Geophys. Res.: Space Phys.*, *84*(A4), 1543–1550. https://doi.org/10.1029/JA084iA04p01543

Xu, J. Y., and Smith, A. K. (2003). Perturbations of the sodium layer: controlled by chemistry or dynamics?. *Geophys. Res. Lett.*, *30*(20), 2056. https://doi.org/10.1029/2003GL018040

Yi, F., Yu, C. M., Zhang, S. D., Yue, X. C., He, Y. J., Huang, C. M., Zhang, Y. P., and Huang, K. M. (2009). Seasonal variations of the nocturnal mesospheric Na and Fe layers at 30°N. *J. Geophys. Res.: Atmos.*, *114*(D1), D01301. https://doi.org/10.1029/2008JD010344

Yuan, T., Feng, W. H., Plane, J. M. C., and Marsh, D. R. (2019). Photochemistry on the bottom side of the mesospheric Na layer. *Atmos. Chem. Phys.*, *19*(6), 3769–3777. https://doi.org/10.5194/acp-19-3769-2019

Yue, X. C., Friedman, J. S., Wu, X. B., and Zhou, Q. H. (2017). Structure and seasonal variations of the nocturnal mesospheric K layer at Arecibo. *J. Geophys. Res.: Atmos. 122*(14), 7260-7275. https://doi.org/10.1002/2017JD026541

Zhao, X. R., Sheng, Z., Shi, H. Q., Weng, L. B., and Liao, Q. X. (2020). Long-term trends and solar responses of the mesopause temperatures observed by SABER during the 2002-2019 Period. *J. Geophys. Res.: Atmos.*, *125*(11), e2020JD032418. https://doi.org/10.1029/2020JD032418

Supplementary Materials for "The low-latitude sodium layer: comparative data from lidarobservations at Hainan, China and São Paulo, Brazil"

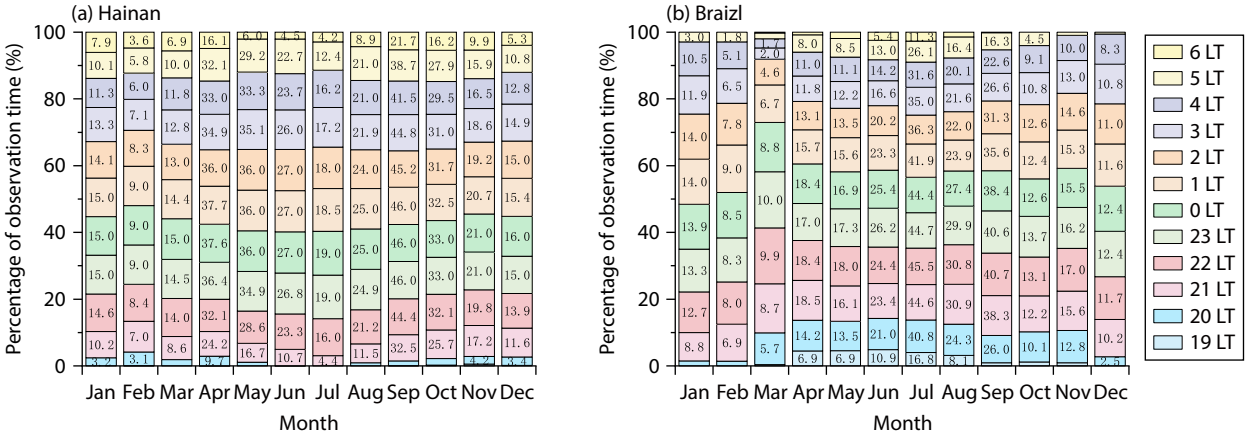

Figure S1. Percentage stacked histograms of observation time per month for (a) Hainan and (b) Brazil. The values in the graph are the total observation time for the corresponding hourly periods.

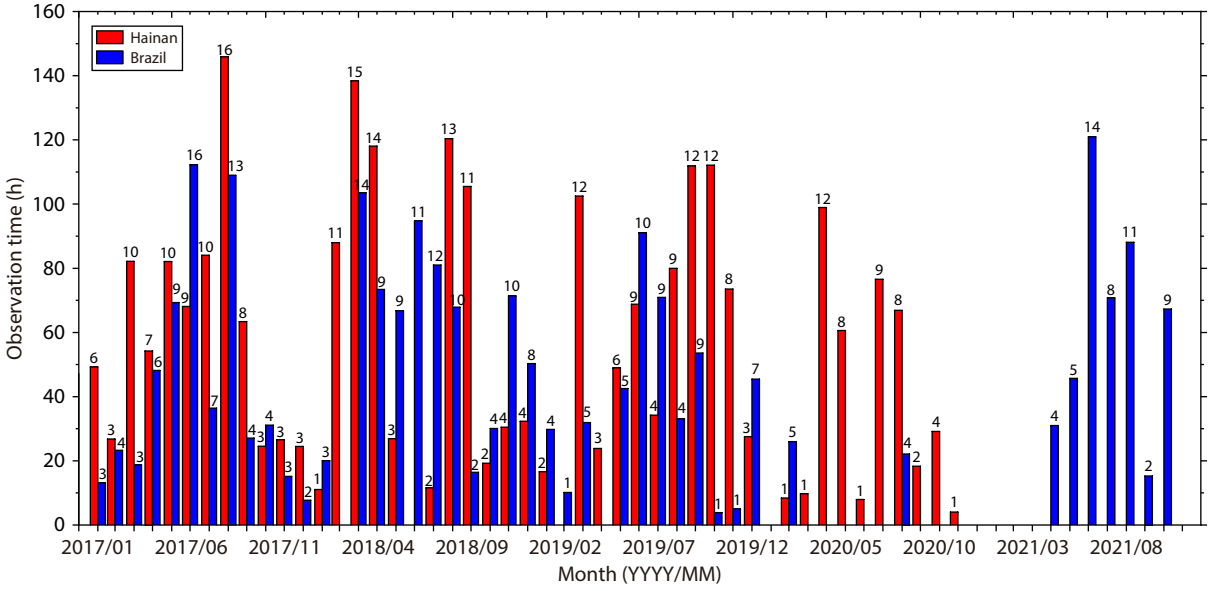

Figure S2. Histograms of the monthly observational hours and nights for each year at Hainan and Brazil.

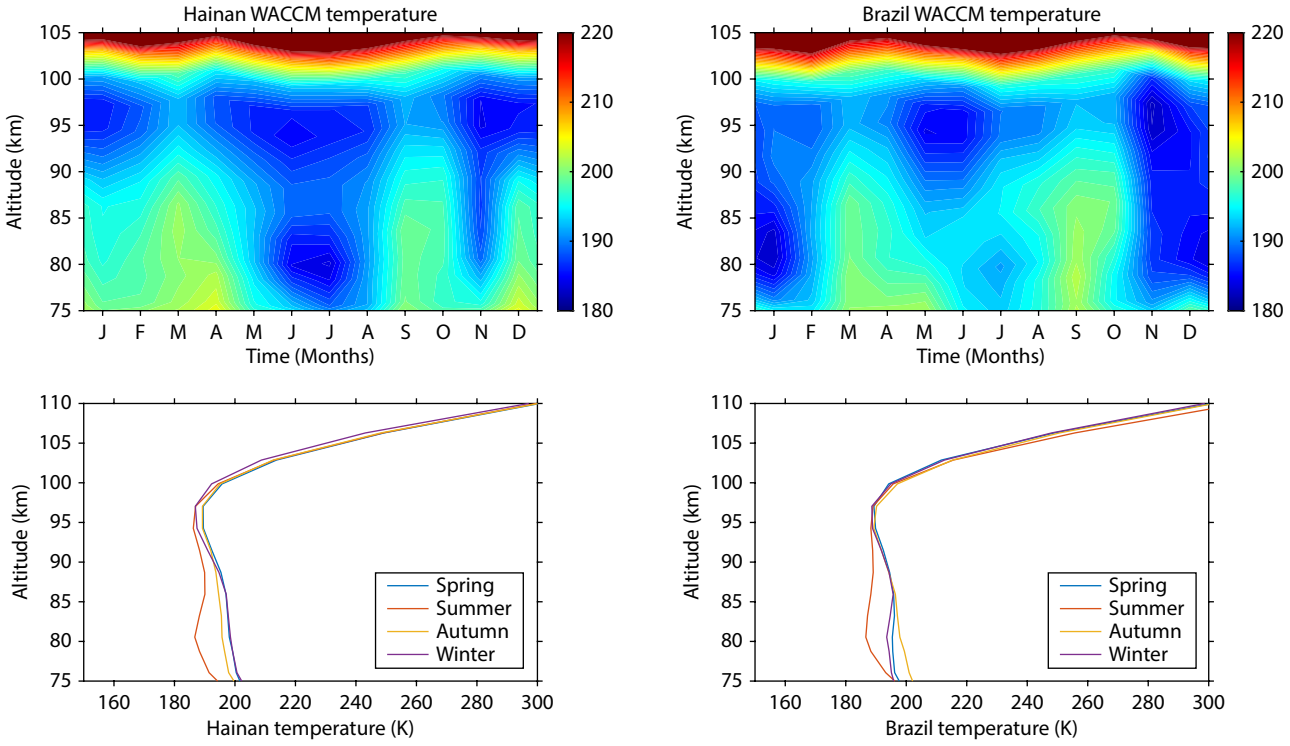

Figure S3. Height profiles of the average temperature simulated by WACCM in different seasons at (a) Hainan and (b) Brazil

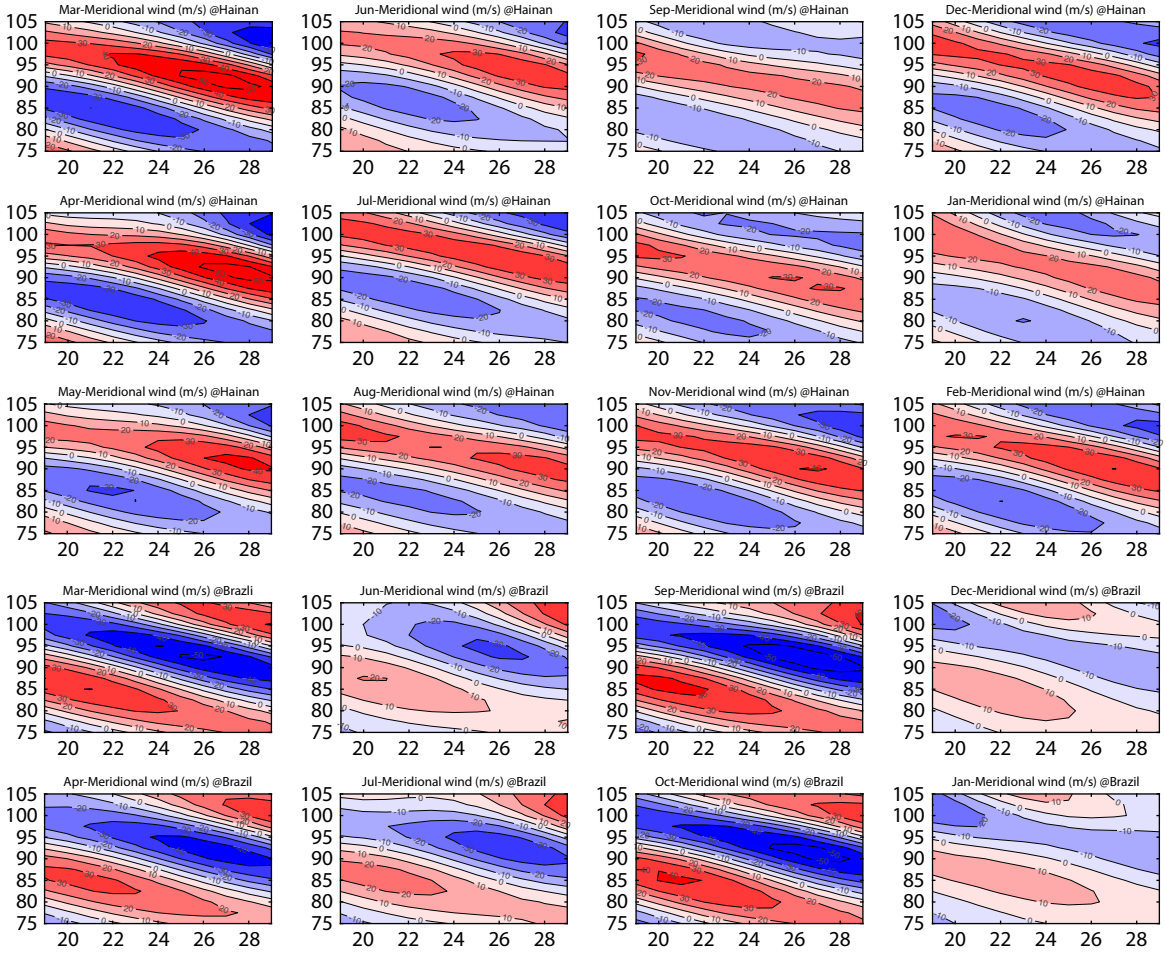

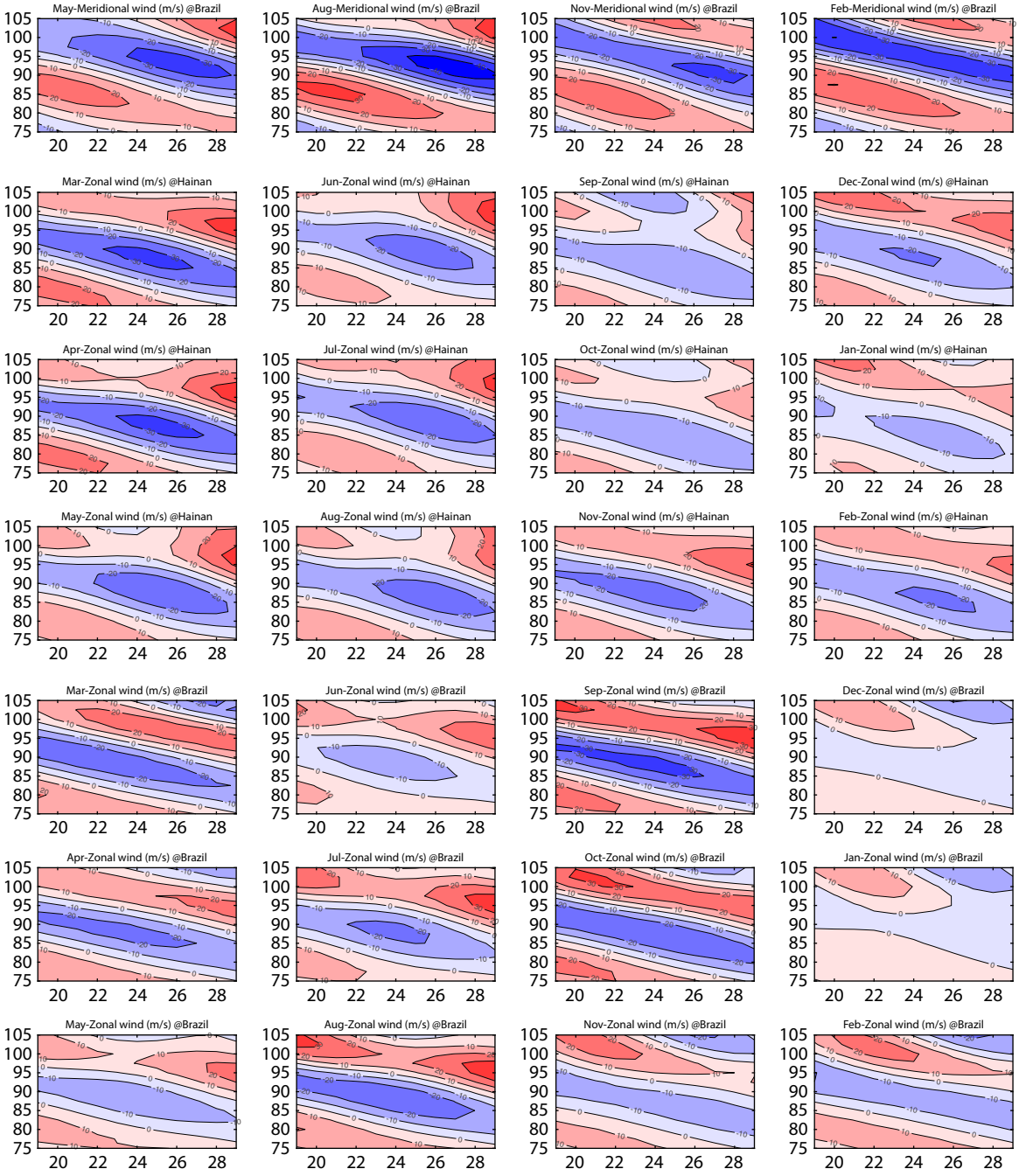

Figure S4. Comparison of monthly mean meridional/zonal wind field reconstructed from CTMT tidal components at Hainan and at Brazil (positive is eastward and northward, respectively).